EXTENSION OF THE SPALART-ALLMARAS ONE-EQUATION TURBULENCE MODEL FOR EFFUSIVE COOLED ROCKET CHAMBERS

R. Hink[1], V. Hannemann[2], T. Eggers[1]
[1]German Aerospace Center, Lilienthalplatz 7,
38108 Braunschweig, Germany
[2]German Aerospace Center, Bunsenstraße 10,
37073 Göttingen, Germany

ABSTRACT

The choice of materials for rocket chamber walls is limited by its thermal resistance. The thermal loads can be reduced substantially by the blowing out of gases through a porous surface [1]. The turbulence models for computational fluid dynamic (CFD) simulations are designed for smooth, non-permeable walls and have to be adjusted to account for the influence of injected fluids. Hink et al. [2] proposed therefore an extension of the Spalart-Allmaras turbulence model [3] for the improved prediction of turbulent boundary layer velocity profiles. In this study the extension is validated against experimental thermal boundary layer data from the Thermosciences Division of the Department of Mechanical Engineering from the Stanford University [4]. All CFD simulations are performed with the finite volume based TAU code of the German Aerospace Center (DLR). Several simulations with different blowing settings were done and discussed in comparison to the results of the original model. Finally, the approach is applied to a two-dimensional simulation of an effusive cooled rocket chamber wall.

1. INTRODUCTION

An accurate prediction of surface temperatures is necessary for an optimal thermal protection design of rocket chamber walls. Several studies have shown the benefit of effusion cooling as cooling technique [5, 6, 7]. Therefore, a short introduction into the current status is given at the beginning of this study. If effusion cooling is used, an accurate prediction of the flow field is necessary, which can be done via the finite volume based TAU code of the German Aerospace Center (DLR). A brief introduction of the laminar flow extensions for the DLR TAU code is given but with respect to effusion cooling in combustion chambers a turbulent flows field is expected. Current implemented one- and two-equation turbulent models at the DLR TAU code are based on the Spalart-Allmaras [3] and Wilcox's k-ω turbulence models [8]. The comparision with the experimental data by Andersen, Kays and Moffat [9] showed that the original turbulence models in combination with the laminar extensions are not sufficient to reproduce the measured velocity profiles. Thus modifications of the turbulence models are necessary for a correct prediction of the turbulent velocity profile, which consequently changes the predict heat transfer or respective surface temperature. Wilcox introduced a revision of the specific-dissipation-rate boundary condition [13] to account for the influence of the effusive medium. Hink et al. [2] proposed an extension of the Spalart-Allmaras turbulence model to predict the correct velocity profile of a turbulent boundary layer on top of effusive permeable wall. The extension is derived from a roughness extension of the Spalart-Allmaras model and the similarity of Wilcox's extensions for effusive and rough walls. Both extensions are implemented in the TAU code and discussed in Hink et al. [2] with respect to the velocity profile.
The aim of this study is to validate the extension of the Spalart-Allmaras model against thermal profile data by Moffat [4]. Furthermore, the necessity is discussed of additional modifications to deal with the thermal boundary layer which are needed in case of rough walls. Therefore, simulations with different blowing ratios and a roughness like extension are performed. Finally, the extended Spalart-Allmaras turbulence model is applied to a generic effusive cooled rocket chamber wall.

2. CURRENT STATUS OF EFFUSION COOLED CHAMBER WALLS

Eckert et al. [14] showed that effusion cooling is more effective than film and convective cooling. Therefore, research was done on micro porous materials which could be used as effusive walls. Metallic porous materials were manufactured by sintering small spheres [15] or wires [16]. The usage of metals is limited to surface temperatures below about 1100 K. The maximum temperature has been increased to 1800 K [17] by the availability of lightweight porous ceramic matrix composites (CMSs) during the last decade [18].
With the development of such thermal resistant materials the demand of accurate design tools arose. In the past many analytical studies were performed to predict the heat flux of effusive cooled walls for example the study of Rannie [19], Rubesin [20] or Kays [21]. Due to the little amount of experimental data for the validation of this different approaches Moffat [4] performed experimental investigations with porous bronze plates. He showed that the approach of Kays, which bases on the approaches of Mickley et al. [22] and Spalding [23], is the most appropriate one in comparison to the experimental results. Kays [24] figured out that the cooling performance is proportional to the specific heat capacity of the coolant gas species. Herbertz [5] showed in detail that effusion cooled thrust chambers provide better performance than actual regenerative cooled ones. Hald et al. [6] presented several results of operational porous C/C rocket chambers up to pressures levels of 8 MPa. An extensive

research of effusive CMCs were conducted in the investigations of Langener [7]. Different experiments were performed with total temperatures up to 750 K, different effusive blowing ratios and different porous CMC materials. He showed also that the assumption of an uniform effusive gas injection is adequate by exit velocity measurements. In addition to Rannie [19] he observed that blowing ratios of F < 0.01 are sufficient for most effusion cooling applications. F is defined there as the ratio between the momentum of the effusive medium and the freestream. Furthermore, an infrared camera was used for the measurement of the temperature distribution on the surface of the effusive CMC.

3. LAMINAR EFFUSION EXTENSIONS FOR THE TAU CODE

The DLR TAU code was extended for effusion cooling problems under laminar flow field conditions by Hannemann [1]. There the effusion mass flux is assumed to enter the computational domain normal to the wall which leaves the tangential velocity components at the respective wall velocity components (zero in case of non-moving walls). The mass balance equation is closed by prescribing the local effusion mass flux. Assuming a subsonic entry of the effusion mass flux at the local wall temperature, the energy balance takes the respective inner energy of the entering fluid into account. Also an assumption about the velocity of the effusion flow has to be made to close the wall normal momentum equation as well as to account for the kinetic energy of the entering fluid in the energy equation. An idealized porous media will let the effusion mass flux enter homogeneously over the complete surface. The effusion velocity can then be calculated as the effusion mass flux divided by the density at the wall which is iterated via the mass balance equation. A higher effusion velocity has to be assumed if the porosity of the surface allows the effusion flux to enter the computational domain only on a fraction of the surface. In all calculations presented here and idealized porous media is assumed (with 100% surface porosity) as well as an adiabatic wall avoiding further terms in the heat flux balance at the surface.

4. TURBULENT VELOCITY PROFILE EXTENSIONS

The laminar effusion extensions are not sufficient in case of an effusion flux entering a turbulent boundary layer calculated with an one or two-equation turbulence model. Wilcox introduced therefore an extension of the boundary condition of the k-ω turbulence model [13]. This extension and the transfer to the one-equation turbulence model of Spalart and Allmaras by Hink [2] is summarized in this chapter after a brief introduction of the turbulent boundary layer velocity profile.

4.1 Boundary layer velocity profile

Velocity profiles of turbulent boundary layers are usually illustrated by plotting the dimensionless velocity $u^+ (= u/u_\tau)$ against the dimensionless wall distance $y^+ (= yu_\tau/\nu)$. These values require the kinematic viscosity $\nu (= \mu/\rho)$ and the friction velocity at the wall u_τ for the nondimensionalization.

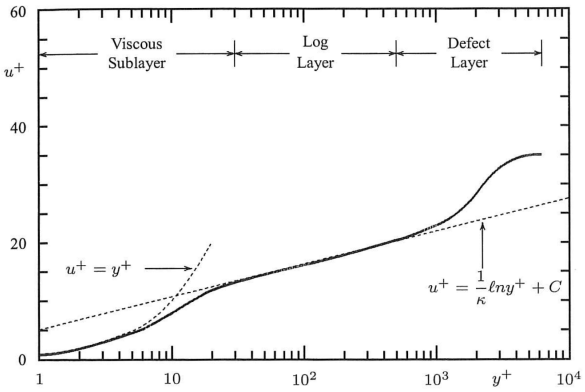

FIG 1. Velocity profile of turbulent boundary layers [13]

The friction velocity is defined as the square root of the wall shear stress τ divided by the fluid density ρ

(1) $u_\tau = \sqrt{\frac{\tau}{\rho}}$.

The u^+-y^+ profile consists of three parts - the laminar sublayer, the logarithmic layer and the defect layer as shown in figure 1. The slope of the profile in the logarithmic layer is mainly determined by the turbulence models. Thus it is the indicator for adequate turbulence modeling.

4.2 Effusion extension by Wilcox

The k-ω turbulence model of Wilcox [8] uses two transport equations. One equation is for the transport of the turbulent kinetic energy k and one for the specific dissipation rate ω. Further details of these equations can be found in Wilcox [8].

Without an effusion extension the slope of the u^+-y^+ profile is overestimated by the k-ω turbulence model in combination with the modifications for the laminar flow. Therefore Wilcox introduces a modification of the specific dissipation rate in the boundary condition at the wall [13]

(2) $\omega = \frac{u_\tau^2}{\nu} S_B$

instead of

(3) $\omega = \frac{6\nu}{\beta_0 d^2}$

with the wall distance d and $\beta_0 = 0.0708$ at a non permeable wall. S_B is the blowing parameter, which is given by

(4) $S_B = \frac{25}{v_w^+(1+5v_w^+)}$.

v_w^+ is the average normal flow velocity through the porous surface scaled by the friction velocity at the surface

(5) $v_w^+ = \frac{v_w}{u_\tau}$.

This boundary condition lowers the specific dissipation rate close to the wall so that the turbulent viscosity increases. The value of the turbulent kinetic energy k is still set to zero at the wall according to Wilcox.

4.3 Roughness extension by Wilcox

The effusion extension of the k-ω turbulence model is similar to a roughness extension. The roughness extension, which is proposed by Wilcox, modifies also the specific dissipation rate in the wall boundary condition [13]

(6) $\omega = \frac{u_\tau^2}{\nu} S_R$.

S_R is the surface roughness parameter, which can be calculated by assuming an average height of sand-grain roughness elements k_r:

(7) $S_R = \frac{100\nu}{u_\tau k_r}$.

4.4 Spalart-Allmaras model

In contrast to the k-ω model, the Spalart-Allmaras turbulence model [3] is a one-equation model which uses a balance equation for a model viscosity

(8) $\frac{\partial \rho\widetilde{\nu}}{\partial t} + \frac{\partial \rho u_i \widetilde{\nu}}{\partial x_i} = P - D + \left[\frac{\partial}{\partial x_i}\left(\frac{\rho\widetilde{\nu}+\rho\nu}{\sigma}\frac{\partial\widetilde{\nu}}{\partial x_i}\right) + \frac{\rho c_{b2}}{\sigma}\left(\frac{\partial\widetilde{\nu}}{\partial x_i}\right)^2\right]$.

In the DLR TAU code this equation is implemented with a variable density as shown in equation 7. The production term P and the destruction term D are formulated as

(9) $P = c_{b1}\rho\widetilde{S}\widetilde{\nu}$

(10) $D = c_{w1} f_w \rho \left(\frac{\widetilde{\nu}}{d}\right)^2$.

The model transport quantity $\widetilde{\nu}$ is related to the kinematic eddy viscosity ν_t as

(11) $\nu_t = \widetilde{\nu} f_{v1}$,

With

(12) $f_{v1} = \frac{\chi^3}{\chi^3+c_{v1}^3}$, with $\chi = \frac{\widetilde{\nu}}{\nu}$.

The total production of turbulence is formulated by a modified magnitude of the vorticity

(13) $\widetilde{S} = S + \frac{\widetilde{\nu}}{\kappa^2 d^2} f_{v2}$, with $f_{v2} = 1 - \frac{\chi}{1+\chi f_{v1}}$.

The magnitude of the vorticity is S in equation 13. The wall-blocking function f_w for the destruction term is shown in equation 14,

(14) $f_w = g\left[\frac{1+c_{w3}^6}{g^6+c_{w3}^6}\right]^{1/6}$.

The limiter function g is formulated as

(15) $g = r + c_{w2}(r^6 - r)$, with $r = \frac{\widetilde{\nu}}{max(\widetilde{S},\varepsilon)\kappa^2 d^2}$.

The wall distance is denoted d. The constant ε = 10^{-16} is used as a limit. The following values are used for the other empirical coefficients above

(16) $\kappa = 0.41, c_{b1} = 0.1355, c_{b2} = 0.622, \sigma = 2/3, c_{w1} = \frac{c_{b1}}{\kappa^2} + \frac{c_{b2}+1}{\sigma}, c_{w2} = 0.3, c_{w3} = 2.0, c_{v1} = 7.1$.

4.5 Boeing roughness extension

The effusion extension of Hink et al. [2] for the Spalart-Allmaras turbulence models is based on the Boeing roughness extension. For this reason the Boeing roughness extension by Aupoix and Spalart [25], which is implemented in the DLR TAU code, is briefly presented here. The roughness extension simulates a higher eddy viscosity near the wall by using an average height of sand-grain roughness elements k_r. This is done by a virtual increase of the wall distance d in the Spalart-Allmaras model

(17) $d = y + d_0(k_r)$.

y is the geometric distance to the wall and $d_0(k_r)$ is a characteristic length of the roughness, which is called roughness length [24]. It can be approximated by the following equation

(18) $d_0(k_r) \approx 0.03 \cdot k_r$.

The function of the variable χ in equation 12 changes with the constant c_{R1} = 0.5 to

(19) $\chi = \frac{\widetilde{\nu}}{\nu} + c_{R1}\frac{k_r}{d}$.

This virtual increase of the wall distance simulates a layer with a higher turbulent viscosity closer to the wall. In the outer part of the boundary layer the virtual increase of the wall distance is much smaller than the geometric wall distance y. For this reason the correction has hardly any influence on the velocity profile there. The Boeing roughness extension proposes also a correction of the wall boundary condition, because it assumes that the sand-grain roughness elements enhance the turbulence at the boundary layer close to the wall.

4.6 Hinks effusion extension

The effusion boundary condition of the k-ω model is similar to the one for roughness. Thus Hink et al. [2] take the approach to compute an effective roughness to account for an effusive wall in the Spalart-Allmaras turbulence model. Therefore, the blowing parameter of equation 4 and the surface roughness parameter of equation 7 are set equal to calculate an effective sand-grain roughness k_r:

(20) $k_r = \frac{\nu v_w^+(4+20v_w^+)}{u_\tau} = \frac{\nu v_w(4+20\frac{v_w}{u_\tau})}{u_\tau^2}$.

The effective roughness can be used for the Boeing roughness extension of Aupoix and Spalart [25] to account for the effusion influence on CFD results origin from the Spalart-Allmaras turbulence model. The extension increases as well as the k-ω extension directly the eddy viscosity close to the wall. A disadvantage of the Spalart-Allmaras effusion extension is that every finite volume of the CFD mesh needs the value of the friction velocity of the respective perpendicular wall cell. The DLR TAU code makes extensive use of parallel computation by splitting the finite volume meshes into several domains. Therewith, additional communication between the domains is needed to pass the friction velocity of the wall to all elements of the mesh above. To bypass this disadvantage the value of u_τ is locally approximated as

(21) $u_{\tau,approx} = \frac{1-C\kappa+\sqrt{(C\kappa-1)^2+4yu\kappa/\nu}}{2y/\nu}$.

This results in an approximation for the effective roughness as shown in equation 22,

(22) $k_r \leq \frac{yv_w(4+20\frac{v_w}{u_{\tau,approx}})}{u}$.

This approximation still underpredicts the effusion extension of the Spalart-Allmaras turbulence model slightly for higher average normal flow velocities, but it calculates values considerable more accurate than the original Spalart-Allmaras turbulence model. Hink et al. also assume that no turbulence is transported by the effusive gas into the boundary layer for the small average normal flow velocity. Thus the eddy viscosity is kept at zero at the wall in contrast to the Boeing roughness extension.

5. TURBULENT THERMAL PROFILE EXTENSIONS FOR ROUGH WALLS

In a simple perfect gas model the thermal conductivity λ can be linked to the dynamic viscosity μ via a constant Prandtl number Pr:

(23) $Pr = \frac{\nu}{a} = \frac{\mu c_p}{\lambda}$.

A constant heat capacity at constant pressure c_p keeps the Pradtl number nondimensional. A similar approach releated the turbulent eddy conductivity λ_t via a turbulent Prandtl number Pr_t:

(24) $Pr_t = \frac{\mu_t c_p}{\lambda_t}$.

Furthermore a nondimensionalized temperature is defined as:

(25) $t^+ = \frac{(t_w - t)\sqrt{\tau/\rho}}{\dot{q}_w/\rho c_p}$.

$\dot{q}_w$ is the surface heat flux and t_w the surface temperature of the wall. In this way a dimensionless turbulent temperature profile can be derived similar to the dimensionless velocity profile:

(26) $t^+ = 13.2Pr + \frac{Pr_t}{\kappa} ln \frac{y^+}{13.2}$.

For further details the literature of Kays and Crawford is referred [24].

5.1 Roughness extension

Additional terms have to be respected for the temperature profile of fully rough surfaces. There the average height of sand-grain roughness elements k_r is larger than the laminar sublayer of the boundary layer so that additional heat transfer between the roughness elements and the wall have to be considered. Furthermore no sublayer exists so that the Pr term of equation 26 can be neglected for typical Prandtl numbers of unity and higher. This results to the nondimensional thermal profile of equation 27 according to Kays and Crawford [24],

(27) $t^+ = \frac{1}{St_r} + \frac{Pr_t}{\kappa} ln \frac{32.6 y^+}{Re_r}$.

The roughness Stanton number St_r is there an additional term in comparison to equation 26, which account for the additional heat transfer by the roughness elements. The roughness Stanton number St_r is defined as shown in equation 28 and need to be measured during experiments,

(28) $St_r = C Re_r^{-m} Pr^{-n}$.

The roughness Reynolds number Re_r of the roughness Stanton number is defined as

(29) $Re_r = \frac{k_r u_\tau}{\nu}$.

The constants were determined during several experiments by Dipprey and Sabersky to C=0.8, m=0.2 and n=0.44 [26].

5.2 Roughness implementation

The additional roughness Stanton number term was implemented in the DLR TAU code by Calvo [27] for an accurate prediction of thermal boundary layer flows at rough walls. There the eddy conductivity is enlarged by a damping function to account for the additional roughness Stanton number term in near wall regions,

(30) $\lambda_t' = \lambda_t [1 - e^{-\frac{y^+}{A_r^+(k_r^+)}}]$.

The polynomial damping function $A_r^+(k_r^+)$ of equation 30 was fitted analytically by a least square procedure over a nondimensional roughness range from zero to 1000. The nondimensional roughness k_r^+ is defined as

(31) $k_r^+ = \frac{k_r u_\tau \rho}{\mu}$.

The result is shown in equation 32,

(32) $A_r^+(k_r^+) = 8.9 + 7.65 \cdot 10^{-2}(k_r^+ - 69.5)^{1.1}$.

For further details the study of Calvo [27] is referred.

6. COMPARISON WITH EXPERIMENTAL DATA

6.1 Configuration and preparation

6.1.1 General settings

The experimental data from the Thermosciences Division of the Stanford University by Moffat [4] is used for the validation of the implemented effusion extensions in the DLR TAU code. During the experiments porous bronze plates were used, which were 0.457 m in width and 0.102 m in length. The experiments were conducted in a wind tunnel 2.44 m in length and 0.152 m in height. The boundary layer was enhanced turbulent from the beginning of the plates. Air was used as fluid in the wind tunnel at a temperature of 293.15 K and as effusive gas. Heat flux measurements over the whole length of the wind tunnel were performed. Furthermore temperature profile measurements were performed. For this study the position x = 2.08 m measured from the beginning of the porous bronze plates is exemplary chosen for the temperature profiles. The measurements were taken at four different average normal flow velocities in addition to measurements without blowing. For each test run the freestream velocity u_∞ and temperature difference $\triangle T$ between the freestream and the effusive were measured which are listed in table 1 and 2 (the heat flux and temperature profile measurements were conducted separately).

TAB 1. Temperature measurement test runs [4]

Test run	$v_w \cdot \rho$ [kg/m^{2}s]	u_∞ [m/s]	$\triangle$T [K]
120266-1	0.000	13.44	18.61
122366-1	0.032	14.13	18.44
122066-1	0.066	14.17	17.39
121966-1	0.133	14.19	16.50

TAB 2. Heat flux measurement test runs [4]

Test run	$v_w \cdot \rho$ [kg/m^{2}s]	u_∞ [m/s]	$\triangle$T [K]
1667-1	0.000	13.25	18.61
1367-1	0.031	13.26	18.44
12966-1	0.063	13.54	18.39
12966-3	0.127	13.60	18.33

The following CFD simulations of the effusive plate are two-dimensional with symmetric boundary conditions. The upstream and downstream farfield extends 3 m in positive and negative x-direction, with symmetry plane boundary conditions on the lower wall between inflow and wall. The upper boundary has a distance of 0.3 m in height. The central scheme is chosen for the spatial discretization for these simulations with the DLR TAU code. The mesh is clustered at the beginning of the effusive plate to resolve the effusive plate tip and the turbulent boundary layer more precisely. The reference temperature of the freestream was

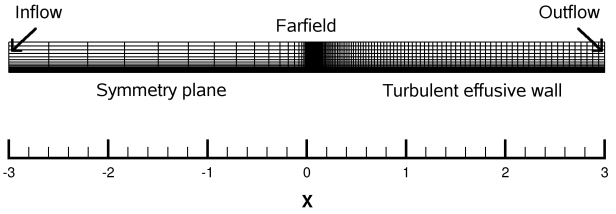

FIG 2. Boundary mapping and mesh

set to 293.15 K and the wall temperature to isothermal with the resulting value of table 1 or 2. A laminar Prandtl number Pr of 0.72 and a laminar to turbulent Prandtl number ratio of 0.8 was chosen here for air as fluid.

6.1.2 Mesh study

For the mesh study five different meshes are tested as summarized in table 3. The coarsest mesh has a y^+ value of 0.08 at the position of the temperature profile data which is used here (x_m = 2.08 m) (at the leading edge $y^+ \approx 1$). Hence these meshes range adequate into the laminar sublayer of this position. The case with the highest average normal flow velocity and the Spalart-Allmaras model without the effusion extension is chosen for the comparison of the meshes because its turbulent eddy viscosity is the smallest and therefore the value of the final density residual is the highest. An error approximation of the temperature profile of the different meshes is performed. For a comparison of this profiles the temperature values in the middle of the turbulent boundary layer with y = 0.005 m ($y^+ \approx 50$) are chosen exemplary. The freestream temperature T_G and the plate temperature T_0 are used for the temperature ratio calculations. The relative error of these temperature ratio values is calculated referring to the Richardson Extrapolation [28] in order to predict the accuracy of each mesh.

TAB 3. Relative error of the meshes in comparison to the Richardson Extrapolation

Number of elements	relative error [%]
approx. 5.000	4.96
approx. 10.000	2.60
approx. 18.000	2.20
approx. 50.000	0.49
approx. 110.000	0.45

An error of less than one percent is of sufficient accuracy considering an error of the experimental data of at least one percent [4]. For this reason the mesh with an element number of approximately 50.000 is chosen (the relative error of the mesh with the Spalart-Allmaras model extension is less than 0.2%).

6.2 Thermal validation of Hinks extension

After the implementation and validation of Hinks effusion extension [2] for the velocity profile, the extension is investigated with respect to experimental temperature profile data of Moffat [4] in figure 3. The resulting temperature profiles are plotted over the wind tunnel height in the same range as the plots of the experimental data by Moffat. The measurement error is less then one percent according to Moffat. The error bars are not shown in this figure because of this small measurement error. The TAU CFD simulations show good agreement with the experimental results and differ only slightly from the experimental values. Especially the almost identical slopes in the logarithmic layer indicate a sufficient modelling. Comparing the temperature profiles illustrated in figure 3 and figure 4, the influence of the velocity profile effusion extension is clearly visible for high blowing rates in the lower part of the boundary layer.
The incorrect velocity profile of the unmodified Spalart-Allmaras model produces inaccurate heat fluxes for the effusion cooled surface. This is shown in figures 5 and 6,

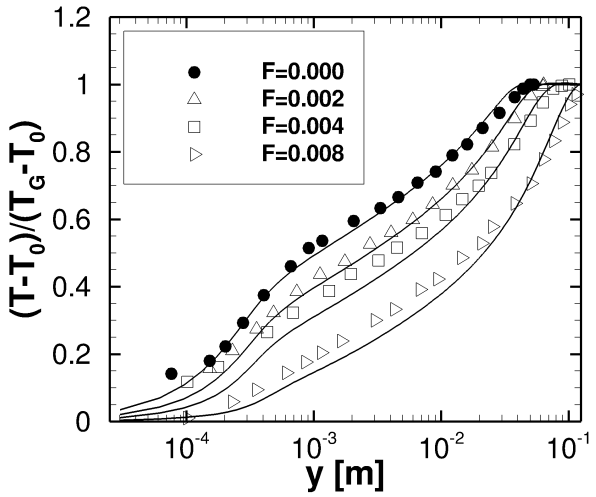

FIG 3. Temperature profiles by the DLR TAU code

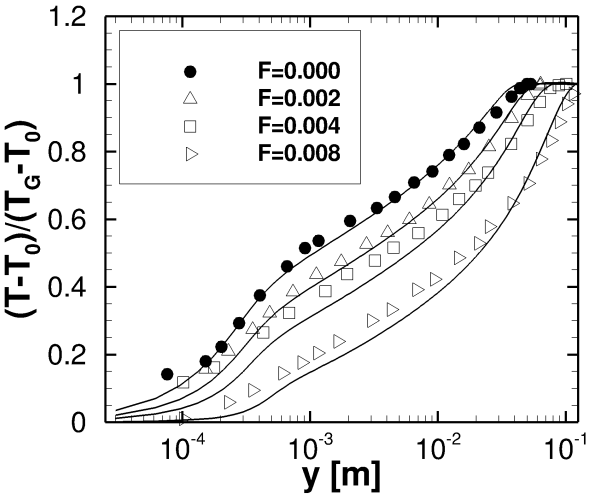

FIG 4. Temperature profiles without extension

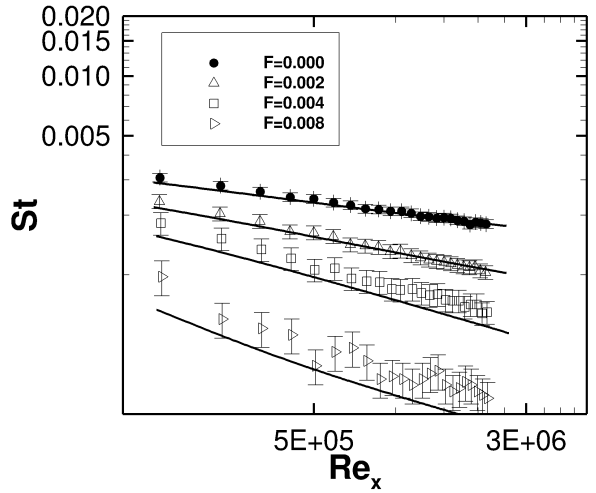

FIG 5. Heat flux measurements

where the heat flux $\dot{q}$ is represented by the nondimensional Stanton number St in comparison to the experimental data of Moffat,

(33) $St = \frac{\dot{q}}{\rho u_\infty c \triangle T}$.

The density ρ and velocity u_∞ and heat capacity c are the freestream values and $\triangle T$ the temperature difference between the freestream and the effusive wall. The Stanton number is plotted over the Reynolds number Re of the plate length x in the same range as the figures of the experimental study,

(34) $Re_x = \frac{\rho u_\infty x}{\nu}$.

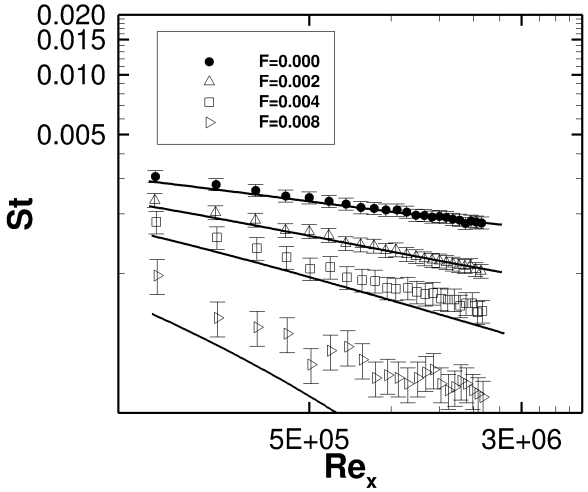

FIG 6. Heat flux without effusion extension

Figure 5 shows the Spalart-Allmaras results with the effusion extension of Hink and figure 6 of the unmodified model. At higher blowing rates the results with the unmodified model differ considerably in comparison to the effusion extended model. Moffat reported also a higher measurement deviation for higher blowing rates. This results from the small absolute heat flux values for the sensor system in comparison to the non or less blowing experiments. For this reason the error bars are shown in these figures for the experimental measurement errors. Overall the effusion extension for the velocity profile shows as well for the temperature profile a more accurate result. Nevertheless, it is investigated if the additional thermal profile extensions for rough walls could further improve the results.

6.3 Comparison with roughness extension

Kays and Crawford [24] remarked that for very rough walls additional extensions have to be respected. For this fully rough walls the average height of sand-grain roughness elements k_r is higher than the laminar sublayer. Thus an additional term have to be considered because additional heat transfer takes place between the roughness elements and the wall. The wall surface is also enlarged and therewith the contact surface for heat transfer. At effusive walls are no additional elements which enlarge the surface. For this reason it is not expected that an additional term is needed or respectively if the roughness extension is applied that heat transfer is overestimated. Andersen et al. [9] remarked also that the effusive plates behave perfect smooth. Nevertheless, it is checked in the following, whether effusive plates show also roughness characteristics for heat transfer and effusive applications. Therefore, the roughness extension of Kays and Crawford [24] is taken with the effective average height of sand-grain roughness elements k_r and the shear stress velocity approximation $u_{\tau,approx}$ of Hink [2]. The results are shown in figure 7. The heat transfer is overestimated with the additional extension. The higher heat transfer coincides with a displaced temperature profile in figure 7. The dimensional values of the heat flux in comparison to the non-blowing and single effusion extension are shown by the Stanton number in figure 8.

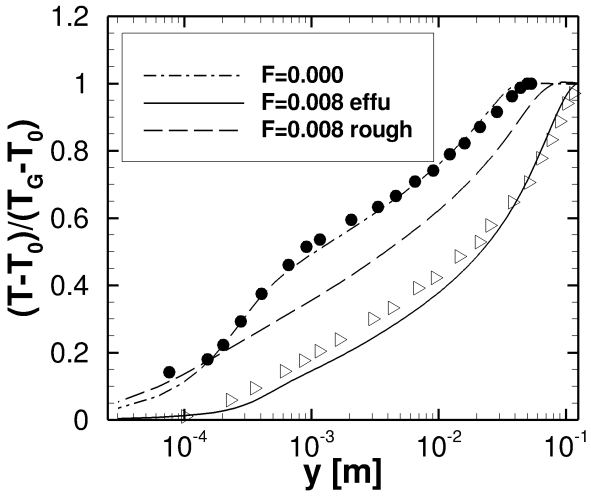

FIG 7. Temperature profile with roughness extension

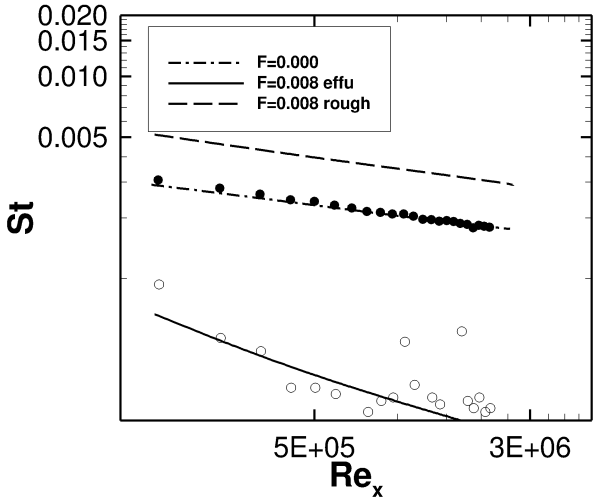

FIG 8. Heat flux with roughness extension

7. EFFUSION EXTENSION APPLIED TO COMBUSTION CHAMBERS

The Keramische Schub-Kammer (KSK, engl. ceramic thrust chamber) project is a DLR project aiming at the development and testing of cheaper, lighter and more reliable cooling concepts for rocket combustion chambers [29]. During the last decade Krenkel [18] developed lightweight porous ceramic matrix composites (CMSs) which enlarged the operation limit of the wall temperature up to 1800 K [17]. Usually temperatures reach more than 3000 K in oxygen-hydrogen rocket combustion chambers. With the assembly of effusion cooled chamber walls temperatures can be lowered below the material limits. Herbertz [5] showed in detail that effusion cooled thrust chambers provide better performance than actual regenerative cooled ones. Hald et al. [6] presented several results of operational porous C/C rocket chambers up to pressures levels of 8 MPa.

7.1 Configuration and preparation of the chamber simulations

7.1.1 General settings

Flow of an oxygen-hydrogen rocket chamber is simplified here to two-dimensional and parallel for comparability with the CFD simulations of the previous chapter. In general effusion cooled rocket chambers are divided in different

effusion cooled segments to adjust the effusion mass flux with the length of the chamber. Here one of such effusion cooled segments is simulated with a parallel freestream. A length of 50 mm is chosen for this effusion cooled segment. The flow is also assumed to be fully turbulent and hydrogen is chosen as effusive medium. The central scheme is chosen for the spatial discretization as in the previous simulations of this study. The composition of the freestream gas with a mixture ratio O/F of 6 is chosen and calculated with the NASA Chemical Equilibrium with Applications (CEA) code [30]. The influence if the turbulence on detailed chemistry is computed with assumed Probability Density Function (PDF). Therefore data of six species is taken from Gaffney et al. [31].

TAB 4. Settings of the chamber simulations

Chamber pressure	20 bar
Mixture ratio	6
Freestream velocity	50 m/s
Mass fractions: H2,H	0.24902, 0.04534
Mass fractions: O2,O	0.00642, 0.00526
Mass fractions: OH,H20	0.05277, 0.64232
Temperature	3672 K
Effusion mass flux	0.025 kg/m^{2}s
Effusive medium	Hydrogen
Effusive temperature	293.15 K

The effusive and non-effusive parts of the wall are assumed to be adiabatic. Additional settings of the CFD simulations are summarized at table 4. A similar mesh study as described in 6.1.2 leads to a number of approximately 100.000 elements. Its error in comparison to the mesh with the double amount of elements is just 0.01%.

7.2 Results

The thermal profiles of the CFD simulations at the middle of the simulated plate x_m are shown in figure 9. The wall temperature T_0 of the effusion cooled simulation is taken for both graphs in this figure.

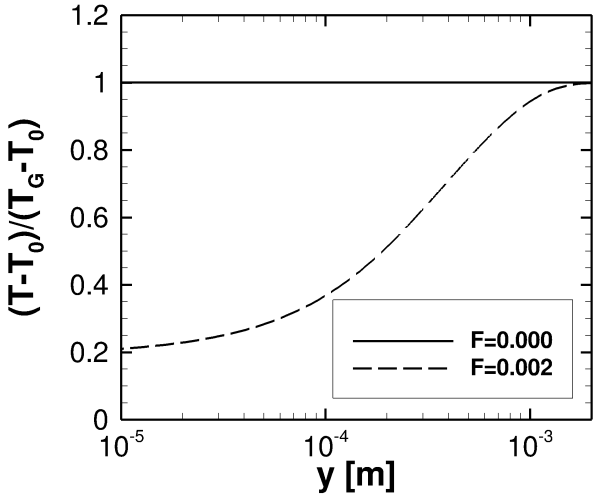

FIG 9. Temperature ratios at point x_m = 0.025 m

For a direct comparison of the temperatures the same graph is plotted with the dimensionalized temperature at figure 10. Already with a blowing ratio of F=0.002 the temperature decrease under the CMC material limit of about 1800 K at x_m.

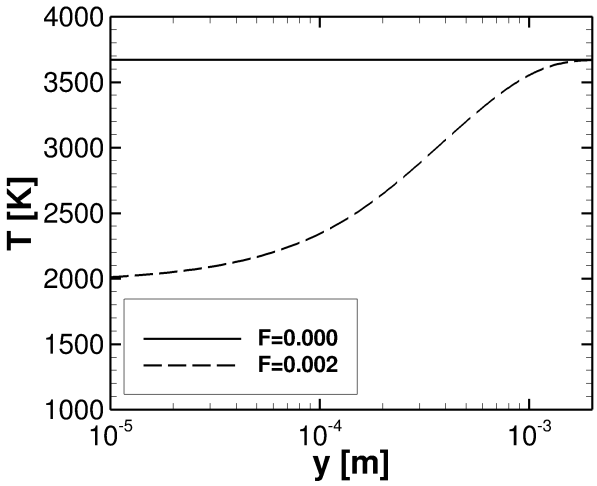

FIG 10. Temperature profile at point x_m = 0.025 m

The resulting temperature along the whole chamber wall is plotted in figure 11. A temperature reduction of more than 25% is shown and the reduction increases in flow direction with the increasing displacement by the effusion mass flux. Nevertheless, the material limit is exceeded at the beginning of the effusive plate. Therefore, higher effusion mass fluxes are necessary at the beginning to stay below the material limit.

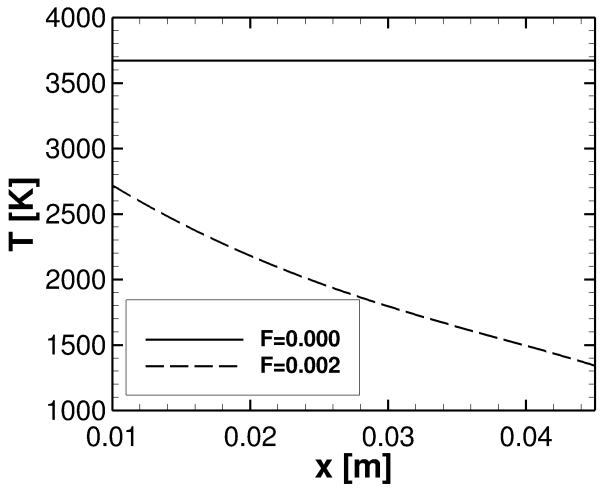

FIG 11. Temperature along the chamber wall

8. CONCLUSION

Hink's effusion extension [2] for turbulent boundary layers was validated with the DLR TAU code for the Spalart-Allmaras turbulence model against experimental data of Moffat [4]. It was shown that no additional extensions like in the case of the roughness extension is needed for an accurate temperature profile prediction on top of the effusive cooled surface. Further investigations are necessary with respect to the turbulent flow prediction in the wake of an effusive cooled surface. Furthermore, the validation and statements are limited to the flow regime of the available data which were taken at low speeds and small temperature differences. The approach was applied to an effusive cooled combustion chamber wall segment. A considerable heat flux reduction even by small effusive mass flows had been shown. Also different effusion mass fluxes can be simulated for different wall segments to reduce the wall temperature to the material limits everywhere.

[1] V. Hannemann, *Numerical investigation of an effusion cooled thermal protection material*, ICCFD4, Ghent, 2006

[2] R. Hink, V. Hannemann, T. Eggers, *Extension of the Spalart-Allmaras One-Equation Turbulence Model for Effusion Cooling Problems*, Deutscher Luft- und Raumfahrtkongress 2013, Stuttgart, 2013

[3] P. R. Spallart, S. R. Allmaras, *A One-Equation Turbulence Model for Aerodynamic Flows*, AIAA-92-0439, 1992

[4] R. J. Moffat, *The Turbulent Boundary Layer on a Porous Plate: Experimental Heat Transfer with Uniform Blowing and Suction*, Department of Mechanical Engineering, Stanford University, Californa, 1967

[5] A. Herbertz, *Numerische Leistungsanalyse von Triebwerksauslegung mit transpirativ gekühlter keramischer Raketenbrennkammer*, Deutsche Gesellschaft für Luft- und Raumfahrt Jahrbuch 2003, München, 2003

[6] H. Hald, M. Ortelt, I. Fischer, D. Greuel and O. Haidn, *Effusion Cooled CMC Rocket Combustion Chamber*, 13th AIAA/CIRA International Space Planes and Hypersonic Systems and Technologies Conference, Capua, Italy, 2005

[7] T. Langener, *A Contribution to Transpiration Cooling of Aerospace Applications Using CMC Walls*, Institute of Aerospace Thermodynamics, University of Stuttgart, Germany, 2011

[8] D. C. Wilcox, W. M. Kays and R. J. Moffat, *Turbulence Modeling for CFD - 2nd Edition*, DCW Industries, La Cañada, California, 1998

[9] P. S. Andersen, W. M. Kays and R. J. Moffat, *The turbulent boundary layer on a porous plate, Report No. HMT-15*, Thermosciences Division, Department of Mechanical Engineering, Stanford University, Stanford, California, 1972

[10] A. Mack, R. Schaefer, B. Esser, A. Guelhan, *Fluid Structure Interaction on a Hypersonic Generic Body-Flap Model*, Proceedings of ICCFD3, Toronto, 2004

[11] A. Mack, R. Schaefer, *Fluid Structure Interaction on a Generic Body-Flap Model in Hypersonic Flow*, AIAA Journal of Spacecraft and Rockets, Vol. 42, No. 5, 2005

[12] A. Mack, *Analyse von heissen Hyperschallstroemungen um Steuerklappen mit Fluid-Struktur Wechselwirkung*, DLR-FB 2005-23 and PhD, TU Braunschweig, 2005

[13] D. C. Wilcox, *Turbulence Modeling for CFD - 3rd Edition*, DCW Industries, La Cañada, California, 2006

[14] E. R. G. Eckert, J. N. B. Livingood, *Report 1182 - Comparison of Effectiveness of Convection-, Transpiration- and Film-Cooling Methods with Air as Coolant*, Lewis Flight Propulsion Laboratory, National Advisore Comittee for Aeronautics, Cleveland, Ohio, 1953

[15] R. Viskanta, L. B. Younis, *Experimental determination of the volumetric heat transfer coefficient between stream of air and ceramic foam*, International Journal of Heat and Mass Transfer, Volume 36, Number 6, 1425-1434, 1993

[16] L. W. Woodruff, G. C. Lorenz, *Hypersonic Turbulent Transpiration Cooling Including Downstream Effects*, AIAA Journal, Vol. 4, No. 6, 1966

[17] M. Bouchez, S. Beyer, *PTAH-SOCAR fuel-cooled composite material structure*, Proceedings of the 15th AIAA International Space Planes and Hypersonic Systems and Technologies Conference, Dayton (Ohio), AIAA 2008-2626, 2008

[18] W. Krenkel, *Entwicklung eines kostengünstigen Verfahrens zur Herstellung von Bauteilen aus keramischen Verbundwerkstoffen*, Dissertation, DLR(German Aerospace Center)-Forschungsbericht 2000-04, Stuttgart, 2000

[19] W. Rannie, *A Simplified Theory of Porous Wall Cooling*, Technical Report, Jet Propulsion Laboratory, Pasadena, California, USA, 1947

[20] M. W. Rubesin, *An Analytical Estimation of the Effect of Transpiration Cooling on the Heat-transfer and Skin-friction Characteristics of a Compressible, Turbulent Boundary Layer*, National Advisory Committee for Aeronautics, Washington, District of Columbia, USA, 1954

[21] W. M. Kays, *Convective Heat and Mass Transfer*, McGraw-Hill Book Company, 1966

[22] H. A. Mickley, R. C. Ross, A. L. Squyers, W. E. Stewart, *Heat, Mass and Momentum Transfer for Flow over a Flat Plate with Blowing or Suction*, National Advisory Committee for Aeronautics, Washington, District of Columbia, USA, 1954

[23] D. B. Spalding, *A Standard Formulation of the Steady Convective Mass Transfer Problem*, International Journal of Heat and Mass Transfer, Volume 1, 1960

[24] W. M. Kays, M. E. Crawford, B. Weigand, *Convective Heat and Mass Transfer*, 4th edition, McGraw-Hill, 2005

[25] B. Aupoix, P. R. Spalart, *Extensions of the Spalart-Allmaras Turbulence Model to Account for Wall Roughness*, International Journal of Heat and Fluid Flow, 24, pp. 454-463, 2003

[26] D. F. Dipprey, R. H. Sabersky, *Heat and Momentum Transfer in Smooth and Rough Tubes at Various Prandtl Numbers*, International Journal of Heat and Mass Transfer, Volume 6, Issue 5, 1963

[27] J. B. Calvo, *Numerical Simulation of Liquid Rocket Engine Cooling Channels*, Department de Mecànica de Fluids, Universitat Politècninca de Catalunya, Deutsches Zentrum für Luft- und Raumfahrt, 2010

[28] M. Hermann, *Numerische Mathematik*, Oldenbourg Wissenschaftsverlag, 2nd Edition, München, 2006

[29] M. Ortelt, A. Herbertz, H. Hald, *Investigations on Fibre Reinforced Combustion Chamber Structures under Effusion Cooled LOX/LH2 Operation*, 45th AIAA/ASME/SAE/ASEE Joint Propulsion Conference and Exhibit, Denver, Colorado, 2009

[30] B. J. McBride, S. Gordon, *Computer Program for Calculation of Complex Chemical Equilibrium Compositions and Applications II. User's Manual and Program Description*, National Aeronautics and Space Administration, Lewis Research Center, Cleveland, Ohio, 1996

[31] R. L. Gaffney, J. A. White, S. S. Girimaji, J. P. Drummond, *Modeling Turbulent Chemistry Interactions Using Assumed PDF Methods*, 28th Joint Propulsion Conference and Exhibit, Nashville, 1992